

Analysis of Charmed Baryon Decays with Strong Phases under SU(3) Symmetry

Jin Sun^{2,*}, Zhi-Peng Xing^{1,†} and Ruilin Zhu^{1‡}

¹*Department of Physics and Institute of Theoretical Physics,
Nanjing Normal University, Nanjing, Jiangsu 210023, China*

²*Particle Theory and Cosmology Group, Center for Theoretical Physics of the Universe,
Institute for Basic Science (IBS), Daejeon 34126, Korea*

The SU(3) analysis is considered a powerful tool in charmed baryon decays. Motivated by recent measurements of anti-triplet charmed baryon two-body decays from the Belle, Belle II, and BESIII Collaborations, we have finally determined the last two IRA form factors, $f^{a'}$ and $g^{a'}$, which were absent in previous work. By considering both real and complex form factor cases in our work, we find that the phases of the form factors are necessary and that complex form factors can explain the experimental data well. Using the fitted form factors, we further numerically study the equivalence of the SU(3) irreducible representation amplitude (IRA) and topological diagrammatic approach (TDA) methods. We find that the IRA and TDA methods can be numerically equivalent with the addition of the new form factors. Based on the conclusions above, and considering some interesting scenarios, the CP violation effects can be predicted in these processes at the order of $O(10^{-3})$. This suggests a promising opportunity to observe CP violation for the first time in charmed baryon decays. Although our predictions depend on some assumptions, considering that the experimental data is far from sufficient to determine CPV through SU(3) analysis, our study is meaningful and instructive for observing CPV at experimental facilities.

I. INTRODUCTION

Over the past 20 years, with an increasing number of measurements by the BESIII, Belle, Belle II, and LHCb collaborations [1–11], charmed baryon decays, as an important part of heavy flavor physics, have attracted increasing attention from both the experimental and theoretical communities [12–22]. Due to the low production threshold, charmed baryons, including singly and doubly charmed baryon decays, have accumulated a significant amount of experimental data. Meanwhile, the rich experimental phenomena in charmed baryon decays face difficulties in perturbative studies because the energy scale is far from the perturbative region. However, the complicated non-perturbative effects also provide an opportunity to study the non-perturbative properties of quantum chromodynamics (QCD). Therefore, charmed baryon decays are a promising platform for studying QCD and precisely testing the Standard Model (SM).

Among the various studies of charmed baryon decays, the SU(3) flavor symmetry analysis, as a non-perturbative method, including the irreducible representation amplitude (IRA) and the topological diagrammatic approach (TDA), is one of the most powerful methods for charmed baryon two-body decays [16, 19, 21–29]. Without detailed dynamical understanding, predictions can be made based on the derived SU(3) relations or global analyses with sufficient experimental data. The quality of the symmetry can be evaluated by how well the known data are explained under the imposed symmetry, as indicated by a good fit quality $\chi^2/\text{d.o.f.}$. As the

simplest type of charmed baryon decays, the anti-triplet charmed baryon two-body decays have accumulated a large amount of experimental data and are therefore the most suitable processes for SU(3) analysis. In previous studies, global fits show that SU(3) flavor symmetry in anti-triplet charmed baryon two-body decays is a good approximation [25]. However, due to the lack of key experimental data, the SU(3) parameters still cannot be fully determined [25]. Therefore, we look forward to additional measurements of key experimental data, which will enable us to conduct deeper and more comprehensive studies.

Fortunately, in 2024, the BESIII Collaboration measured the decay branching ratios of Λ_c^+ , while the Belle and Belle II Collaborations measured the decay branching ratios and asymmetry parameters of Ξ_c^0 for the first time [30–32], as well as the decay branching ratios of Ξ_c^+ [33] as

$$\begin{aligned} Br(\Lambda_c^+ \rightarrow p\pi^0) &= (0.0156_{-0.0058}^{+0.0072} \pm 0.002)\%, \\ Br(\Lambda_c^+ \rightarrow p\eta) &= (0.163 \pm 0.031 \pm 0.011)\%, \\ Br(\Lambda_c^+ \rightarrow pK_L) &= (1.67 \pm 0.06 \pm 0.04)\%, \\ Br(\Xi_c^0 \rightarrow \Xi^0\pi^0) &= (0.69 \pm 0.03 \pm 0.05 \pm 0.13)\%, \\ Br(\Xi_c^0 \rightarrow \Xi^0\eta) &= (0.16 \pm 0.02 \pm 0.02 \pm 0.03)\%, \\ Br(\Xi_c^0 \rightarrow \Xi^0\eta') &= (0.12 \pm 0.03 \pm 0.01 \pm 0.02)\%, \\ Br(\Xi_c^+ \rightarrow pK_S^0) &= (7.16 \pm 0.46 \pm 0.20 \pm 3.21) \times 10^{-4}, \\ Br(\Xi_c^+ \rightarrow \Lambda\pi^+) &= (4.52 \pm 0.41 \pm 0.26 \pm 2.03) \times 10^{-4}, \\ Br(\Xi_c^+ \rightarrow \Sigma^0\pi^+) &= (1.20 \pm 0.08 \pm 0.07 \pm 0.54) \times 10^{-3}, \\ \alpha(\Xi_c^+ \rightarrow \Xi^0\pi^0) &= -0.90 \pm 0.15 \pm 0.23. \end{aligned} \quad (1)$$

Based on the new measurements, all SU(3) IRA amplitudes can now be determined, enabling a deeper understanding of the weak interactions in charmed particle decays, including potential CP violation (CPV) effects.

* sunjin0810@ibs.re.kr

† zpxing@nnu.edu.cn (corresponding author)

‡ rlzhu@nynu.edu.cn

CP violation (CPV) is a fundamental topic in particle physics [28, 34–47], as it is necessary to explain the baryon-antibaryon asymmetry in the universe. However, CP violation has only been observed in meson decays, and no definitive evidence of CP violation in baryon decays has been reported in particle physics experiments. Current observations of CP violation are insufficient to explain the matter-antimatter asymmetry of the universe, underscoring the importance of searching for new sources of CP violation. In the general theoretical framework of CP violation presented in Ref. [48], the direct CP violation in two-body decay processes is proportional to the product of the weak phase difference and the strong phase difference: $A_{CP} \propto \sin(\phi_1 - \phi_2) \sin(\delta_1 - \delta_2)$. Here, δ_i represents the strong phase, while ϕ_i denotes the weak phase originating from the CKM matrix elements. Under SU(3) symmetry, the strong phase within an SU(3) amplitude corresponding to different channels is identical. With sufficient experimental data, the strong phases of anti-triplet charmed baryon decays can be determined. Consequently, CP violation can also be incorporated into these processes.

This paper is organized as follows: In Section II, we present a global analysis of anti-triplet charmed baryon two-body decays using the IRA method. Section III utilizes the topological diagrams to gain a comprehensive understanding of SU(3) symmetry. By determining the previously undetermined parameters from prior work [25], we further numerically investigate the equivalence between the IRA and TDA methods. Subsequently, the strong phase is incorporated into the form factor that constitutes the SU(3) amplitude, with determined values that carry large uncertainties. The determined strong phases motivate us to explore CPV in these processes. In Section IV, CPV is expressed using the SU(3) amplitude with contributions from two sources of weak and strong phases under specific scenarios. The conclusions are presented in Section V.

II. THE GLOBAL ANALYSIS OF ANTI-TRIPLET CHARMED BARYON TWO-BODY DECAYS WITH IRA

Using SU(3) flavor symmetry, the anti-triplet charmed baryon, light baryon octet, and light meson octet can be expressed by 3×3 matrices $T_{c\bar{3}}$, T_8 , and P , respectively [25] as

$$T_{c\bar{3}} = \begin{pmatrix} 0 & \Lambda_c^+ & \Xi_c^+ \\ -\Lambda_c^+ & 0 & \Xi_c^0 \\ -\Xi_c^+ & -\Xi_c^0 & 0 \end{pmatrix}, P = \begin{pmatrix} \frac{\pi^0 + \eta_q}{\sqrt{2}} & \pi^+ & K^+ \\ \pi^- & \frac{-\pi^0 + \eta_q}{\sqrt{2}} & K^0 \\ K^- & \bar{K}^0 & \eta_s \end{pmatrix},$$

$$T_8 = \begin{pmatrix} \frac{\Sigma^0}{\sqrt{2}} + \frac{\Lambda^0}{\sqrt{6}} & \Sigma^+ & p \\ \Sigma^- & -\frac{\Sigma^0}{\sqrt{2}} + \frac{\Lambda^0}{\sqrt{6}} & n \\ \Xi^- & \Xi^0 & -\frac{2\Lambda^0}{\sqrt{6}} \end{pmatrix}. \quad (2)$$

Here the anti-triplet charmed baryon can also be expressed as $(T_{c\bar{3}})_i = \epsilon^{ijk}(T_{c\bar{3}})^{[jk]} = (\Xi_c^0, -\Xi_c^+, \Lambda_c^+)$, and the η_s and η_q are the mixture of η_1 and η_8 : $\eta_s = \eta_q/\sqrt{3} - \eta_8\sqrt{2}/\sqrt{3}$, $\eta_1 = \eta_q\sqrt{2}/\sqrt{3} + \eta_8/\sqrt{3}$. To analyze the experimental data, we consider the physical mixing effects with $\eta^{(\prime)}$ states

$$\begin{pmatrix} \eta \\ \eta' \end{pmatrix} = \begin{pmatrix} \cos \phi & -\sin \phi \\ \sin \phi & \cos \phi \end{pmatrix} \begin{pmatrix} \eta_q \\ \eta_s \end{pmatrix}, \quad (3)$$

where the physical mixing angles $\phi = (39.3 \pm 1.0)^\circ$ [49].

With these defined matrices, the SU(3)-invariant decay amplitudes for anti-triplet charmed baryon two-body decays can be expressed as $a_{15} \times \epsilon_{imn}(T_{c\bar{3}})^{[mn]}(H_{15})_j^{\{ik\}}(\bar{T}_8)_k^j P_l^i$ and $a_6 \times (T_{c\bar{3}})^{[ik]}(H_6)_{\{ij\}}(\bar{T}_8)_k^j P_l^i$. Here the $H_{15,6}$ is the decomposed matrix element of the effective weak interaction Hamiltonian. In the IRA method, the four-Fermi effective Hamiltonian, such as $c \rightarrow s\bar{d}u$, $c \rightarrow s\bar{s}u$, or $c \rightarrow u\bar{q}q$, is decomposed as $3 \otimes \bar{3} \otimes 3 = 3 \oplus 3 \oplus \bar{6} \oplus 15$. The detailed decomposition formula can be found in Ref. [50]. The nonzero matrices are H_6 and H_{15} . By enumerating all possible matrix combinations, nine independent amplitudes can be constructed as follows:

$$\begin{aligned} \mathcal{M}^{IRA} = & a_{15} \times (T_{c\bar{3}})_i (H_{15})_j^{\{ik\}} (\bar{T}_8)_k^j P_l^i \\ & + b_{15} \times (T_{c\bar{3}})_i (H_{15})_j^{\{ik\}} (\bar{T}_8)_k^l P_l^j \\ & + c_{15} \times (T_{c\bar{3}})_i (H_{15})_j^{\{ik\}} (\bar{T}_8)_l^j P_k^l \\ & + d_{15} \times (T_{c\bar{3}})_i (H_{15})_l^{\{jk\}} (\bar{T}_8)_j^l P_k^i \\ & + e_{15} \times (T_{c\bar{3}})_i (H_{15})_l^{\{jk\}} (\bar{T}_8)_j^i P_k^l \\ & + a_6 \times (T_{c\bar{3}})^{[ik]} (H_6)_{\{ij\}} (\bar{T}_8)_k^j P_l^i \\ & + b_6 \times (T_{c\bar{3}})^{[ik]} (H_6)_{\{ij\}} (\bar{T}_8)_k^l P_l^j \\ & + c_6 \times (T_{c\bar{3}})^{[ik]} (H_6)_{\{ij\}} (\bar{T}_8)_l^j P_k^l \\ & + d_6 \times (T_{c\bar{3}})^{[ik]} (H_6)_{\{ij\}} (\bar{T}_8)_k^i P_l^j. \end{aligned} \quad (4)$$

Here $(a - e)_{15,6}$ means the corresponding SU(3) amplitudes. Using these nine SU(3) amplitudes, all amplitudes of anti-triplet charmed baryon two-body decays can be expressed. The specific formulas for these amplitudes can be found in Ref. [25].

To correctly describe the phenomenological results of anti-triplet charmed baryon two-body decays, each SU(3) amplitude can be expressed by parity-violating form factors $f_{6,15}^{b,c,d}, f^{a(\prime)}$ and parity-conserving form factors $g_{6,15}^{b,c,d}, g^{a(\prime)}$ as

$$\begin{aligned} q_6 &= G_F \bar{u}(f_6^q - g_6^q \gamma_5)u, \quad q = a, b, c, d, \\ q_{15} &= G_F \bar{u}(f_{15}^q - g_{15}^q \gamma_5)u, \quad q = a, b, c, d, e. \end{aligned} \quad (5)$$

Subsequently, the branching ratios and polarization

parameters α , β and γ are expressed as

$$\begin{aligned} \frac{d\Gamma}{d\cos\theta_M} &= \frac{G_F^2 |\vec{p}_{B_n}| (E_{B_n} + M_{B_n})}{8\pi M_{B_c}} (|F|^2 + \kappa^2 |G|^2) \\ &\quad \times (1 + \alpha \hat{\omega}_i \cdot \hat{p}_{B_n}), \\ \alpha &= \frac{2\text{Re}(F * G)\kappa}{(|F|^2 + \kappa^2 |G|^2)}, \quad \beta = \frac{2\text{Im}(F * G)\kappa}{(|F|^2 + \kappa^2 |G|^2)}, \\ \gamma &= \frac{|F|^2 - |\kappa G|^2}{(|F|^2 + \kappa^2 |G|^2)}, \quad \kappa = \frac{|\vec{p}_{B_n}|}{(E_{B_n} + M_{B_n})}. \end{aligned} \quad (6)$$

Note that most of the experimental data involving η and η' contain the combination $a_6 - a_{15}$, except for the $\Xi_c^0 \rightarrow \Xi^0 \eta$ and $\Xi_c^0 \rightarrow \Xi^0 \eta'$ processes, which involve the combination $a_6 + a_{15}$, as shown in Tables II and III of Ref. [25]. It is expected that the amplitudes a_6 and a_{15} will have large uncertainties because only the combination $a_6 - a_{15}$ can be determined precisely. To account for this uncertainty, we redefine the new SU(3) irreducible amplitudes and corresponding form factors as follows:

$$\begin{aligned} f^a &= f_6^a - f_{15}^a, & g^a &= g_6^a - g_{15}^a \\ f^{a'} &= f_6^a + f_{15}^a, & g^{a'} &= g_6^a + g_{15}^a. \end{aligned} \quad (7)$$

The previous experimental data can determine the parameter a with precision, but not a' [25]. Fortunately, the amplitudes from the newly measured processes, $\Xi_c^0 \rightarrow \Xi^0 \eta^{(\prime)}$, depend on a' . This means that the corresponding form factors $f^{a'}$ and $g^{a'}$ can be obtained, which were absent in previous work. Therefore, it is imperative to revisit the global analysis of anti-triplet charmed baryon two-body decays based on these latest results.

By assuming real form factors for simplicity, we perform fits using the updated data from Eq. 1 and the latest PDG [48] in Table I using the nonlinear least- χ^2 method [51]. Here, we disregard the BESIII result $\alpha(\Lambda_c^+ \rightarrow \Xi^0 K^+) = 0.01 \pm 0.16 \pm 0.03$ [52], which has a large error compared to the central value and is inconsistent with our previous work [25]. In our preliminary analysis, the channels $\Xi_c^0 \rightarrow \Xi^0 \pi^0$ and $\Xi_c^+ \rightarrow \Sigma^0 \pi^+$ contribute the most to the χ^2 . The situation we encountered of $\Xi_c^0 \rightarrow \Xi^0 \pi^0$ is same with previous work [46], while the measurement of the branching ratio for $\Xi_c^+ \rightarrow \Sigma^0 \pi^0$ is in conflict with previous predictions [25, 29, 46].

Therefore, we attempt to exclude these measurements from the global fit and present the fit results (Case I) in Table II. Note that the new measurements of the three channels $\Xi_c^+ \rightarrow p K_S$, $\Xi_c^+ \rightarrow \Lambda^0 \pi^+$, and $\Xi_c^+ \rightarrow \Sigma^0 \pi^+$ are obtained through the ratio $Br(\Xi_c^+ \rightarrow T_8 P)/Br(\Xi_c^+ \rightarrow \Xi^- 2\pi^+)$. The large uncertainty of $Br(\Xi_c^+ \rightarrow \Xi^- 2\pi^+) = (2.9 \pm 1.3)\%$ will increase the uncertainty in these three measurements naturally. However, the ratios $Br(\Xi_c^+ \rightarrow p K_S)/Br(\Xi_c^+ \rightarrow \Lambda^0 \pi^+)$ and $Br(\Xi_c^+ \rightarrow \Lambda^0 \pi^+)/Br(\Xi_c^+ \rightarrow \Sigma^0 \pi^+)$ can effectively eliminate the uncertainty from $Br(\Xi_c^+ \rightarrow \Xi^- 2\pi^+)$. In the fit of Case I, we find that these predicted ratios differ significantly from the experimental data in Table. I. Based on the fitted results, $Br(\Xi_c^+ \rightarrow p K_S) = 0.144(14)$,

$Br(\Xi_c^+ \rightarrow \Lambda^0 \pi^+) = 0.0218(32)$, $Br(\Xi_c^+ \rightarrow \Sigma^0 \pi^+) = 0.3161(88)$, these ratios are predicted as

$$\begin{aligned} \frac{Br(\Xi_c^+ \rightarrow p K_S)}{Br(\Xi_c^+ \rightarrow \Lambda^0 \pi^+)} &= 6.6 \pm 1.2, \\ \frac{Br(\Xi_c^+ \rightarrow \Lambda^0 \pi^+)}{Br(\Xi_c^+ \rightarrow \Sigma^0 \pi^+)} &= 0.069 \pm 0.010. \end{aligned} \quad (8)$$

This also suggests that the assumption of a real form factor no longer aligns with the current experimental data.

In our result (Case I), we predict $\alpha(\Lambda_c^+ \rightarrow \Sigma^0 K^+) = -0.9960 \pm 0.0042$, which deviates by 2σ from the experimental data $\alpha(\Lambda_c \rightarrow \Sigma^0 K^+)_{\text{exp}} = -0.54 \pm 0.20$. The value $\alpha(\Lambda_c^+ \rightarrow \Xi^0 K^+) = 0.957 \pm 0.018$ also conflicts with the experimental measurement $\alpha(\Lambda_c^+ \rightarrow \Xi^0 K^+)_{\text{exp}} = 0.01 \pm 0.16 \pm 0.03$. These conflicting polarization parameter data indicate that the assumption of real form factors is insufficient, as α is proportional to $\text{Re}(F * G)$ which is highly dependent on the complex phase of the form factors F and G .

The above analysis demonstrates that the strong phase of the form factors defined in Eq. 5 is essential. We can decompose these form factors into their absolute values and phases as follows:

$$\begin{aligned} f_6^q &= |f_6^q| e^{i\delta f_6^q}, & g_6^q &= |g_6^q| e^{i\delta g_6^q}, & q &= a, b, c, d, \\ f_{15}^q &= |f_{15}^q| e^{i\delta f_{15}^q}, & g_{15}^q &= |g_{15}^q| e^{i\delta g_{15}^q}, & q &= a, b, c, d, e. \end{aligned} \quad (9)$$

Before conducting our global analysis, the degrees of freedom can be calculated using the formula $d.o.f = N - M + 1$, where $N = 37$ represents the number of experimental data points, and M is the number of parameters used in the analysis. Note that the ratios $Br(\Xi_c^+ \rightarrow p K_S)/Br(\Xi_c^+ \rightarrow \Lambda^0 \pi^+)$ and $Br(\Xi_c^+ \rightarrow \Lambda^0 \pi^+)/Br(\Xi_c^+ \rightarrow \Sigma^0 \pi^+)$ are adopted to reduce the uncertainty rather than the respective branching ratios. Since we introduce 18 form factors in our analysis, and each form factor consists of its absolute value and phase, the total number of parameters, M , can be calculated as $M = 18 \times 2 - 1$, after subtracting the global phase and setting $\delta f_6^a = 0$. The degrees of freedom (d.o.f) in this fit is $37 - 35 + 1 = 3$. The small d.o.f suggests that the experimental data is insufficient to precisely determine the strong phase, leading to large uncertainties in the fit results.

After including all 35 parameters in our global fit, we derive the numerical results of form factors presented in Table II (case II), with a $\chi^2/d.o.f = 1.36$. However, we find that the complex form still struggles to simultaneously explain the new measurements $\Xi_c^+ \rightarrow p K_S$, $\Xi_c^+ \rightarrow \Lambda^0 \pi^+$, and $\Xi_c^+ \rightarrow \Sigma^0 \pi^+$. While their individual ratios can be fitted accurately, more precise experimental data on $Br(\Xi_c^+ \rightarrow \Xi^- 2\pi^+)$ is required to obtain the accurate respective branching ratios in the future.

The low $\chi^2/d.o.f$ indicates that the SU(3) symmetry is a reliable and effective symmetry, as it fits the experimental data well. The predictions (case II) calculated using the fitted complex 18 form factors are shown in Table. III and Table. IV. One can find that the added phase

TABLE I: Experimental data and fitting results of anti-triplet charmed baryons two-body decays for two different fits. Case I(II)[III] means the fit results for the real(complex)[new] form factors.

channel	exp		Case I		Case II		Case III	
	Br(%)	α	Br(%)	α	Br(%)	α	Br(%)	α
$\Lambda_c^+ \rightarrow p\pi^0$	0.0156(75)		0.0163(60)		0.0158(75)		0.0141(65)	
$\Lambda_c^+ \rightarrow pK_S^0$	1.59(7)	0.2(5)	1.581(47)	0.39(14)	1.580(69)	-0.05(38)	1.584(48)	0.15(24)
$\Lambda_c^+ \rightarrow pK_L^0$	1.67(7)		1.689(49)		1.677(69)		1.690(51)	
$\Lambda_c^+ \rightarrow p\eta$	0.158(11)		0.1583(97)		0.158(11)		0.154(11)	
$\Lambda_c^+ \rightarrow p\eta'$	0.0484(91)		0.0484(61)		0.0488(91)		0.0505(74)	
$\Lambda_c^+ \rightarrow \Lambda\pi^+$	1.29(5)	-0.755(6)	1.309(47)	-0.7536(60)	1.272(48)	-0.7551(60)	1.270(48)	-0.7551(60)
$\Lambda_c^+ \rightarrow \Sigma^0\pi^+$	1.27(6)	-0.466(18)	1.248(46)	-0.472(15)	1.245(48)	-0.472(15)	1.246(48)	-0.472(15)
$\Lambda_c^+ \rightarrow \Sigma^+\pi^0$	1.24(9)	-0.484(27)	1.262(46)	-0.470(15)	1.253(48)	-0.471(15)	1.257(48)	-0.471(15)
$\Lambda_c^+ \rightarrow \Xi^0 K^+$	0.55(7)	0.01(16)	0.423(29)		0.555(70)	0.04(15)	0.558(68)	0.05(13)
$\Lambda_c^+ \rightarrow \Lambda^0 K^+$	0.0642(31)	-0.58(5)	0.0639(29)	-0.547(44)	0.0645(31)	-0.585(49)	0.0644(31)	-0.588(48)
$\Lambda_c^+ \rightarrow \Sigma^+\eta$	0.32(5)	-0.99(6)	0.299(47)	-0.989(29)	0.32(5)	-0.985(60)	0.338(49)	-0.982(59)
$\Lambda_c^+ \rightarrow \Sigma^+\eta'$	0.41(8)	-0.460(67)	0.428(66)	-0.467(64)	0.407(80)	-0.460(67)	0.380(68)	-0.443(64)
$\Lambda_c^+ \rightarrow \Sigma^0 K^+$	0.0370(31)	-0.54(20)	0.0377(18)	-0.9960(42)	0.0389(25)	-0.58(16)	0.0386(25)	-0.58(14)
$\Lambda_c^+ \rightarrow n\pi^+$	0.066(13)		0.0642(23)		0.0766(88)		0.0765(78)	
$\Lambda_c^+ \rightarrow \Sigma^+ K_S^0$	0.047(14)		0.0277(27)		0.042(13)		0.0323(43)	
$\Xi_c^+ \rightarrow \Xi^0\pi^+$	1.6(8)		0.875(77)		1.94(59)		2.02(32)	
$\Xi_c^+ \rightarrow pK_S$	0.0716(325)		0.144(14)					
$\Xi_c^+ \rightarrow \Lambda^0\pi^+$	0.0452(209)		0.0218(32)					
$\Xi_c^+ \rightarrow \Sigma^0\pi^+$	0.120(55)		0.3161(88)					
$\frac{\Xi_c^+ \rightarrow pK_S}{\Xi_c^+ \rightarrow \Lambda^0\pi^+}$	1.58(21)				1.62(20)		1.51(18)	
$\frac{\Xi_c^+ \rightarrow \Lambda^0\pi^+}{\Xi_c^+ \rightarrow \Sigma^0\pi^+}$	0.378(52)				0.375(45)		0.352(39)	
$\Xi_c^0 \rightarrow \Lambda K_S^0$	0.32(6)		0.225(34)		0.324(60)		0.345(57)	
$\Xi_c^0 \rightarrow \Xi^-\pi^+$	1.43(27)	-0.640(51)	1.16(18)	-0.709(45)	1.18(19)	-0.640(51)	1.17(18)	-0.640(51)
$\Xi_c^0 \rightarrow \Xi^- K^+$	0.039(11)		0.0515(80)		0.0491(82)		0.0508(81)	
$\Xi_c^0 \rightarrow \Sigma^0 K_S^0$	0.054(16)		0.054(16)		0.055(16)		0.056(16)	
$\Xi_c^0 \rightarrow \Sigma^+ K^-$	0.18(4)		0.195(39)		0.181(40)		0.183(40)	
$\Xi_c^0 \rightarrow \Xi^0\pi^0$	0.69(14)	-0.90(28)	0.152(48)	-0.45(13)	0.68(14)	-0.87(28)	0.60(11)	-0.87(26)
$\Xi_c^0 \rightarrow \Xi^0\eta$	0.16(4)		0.16(4)		0.16(4)		0.159(40)	
$\Xi_c^0 \rightarrow \Xi^0\eta'$	0.12(4)		0.12(4)		0.12(4)		0.126(40)	

of the form factor can perfectly explain the anomaly in the polarization parameter $\alpha(\Lambda_c \rightarrow \Sigma^0 K^+)$ and branching ratios $Br(\Xi_c^0 \rightarrow \Xi^0 \pi^0)$. However, as expected, the uncertainty in the absolute value and phase is very large, which reduces the predictive power of our results. Therefore, we still look forward to more experimental data to reduce the uncertainty in our results.

III. THE COMPREHENSIVE ANALYSIS OF ANTI-TRIPLET CHARMED BARYON TWO BODY DECAYS WITH THE EQUIVALENCE OF TDA AND IRA

In the above analysis, all nine IRA amplitudes and the 18 associated form factors are determined based on the key experimental results measured by Belle and Belle

II, as shown in Table II. This facilitates a detailed and comprehensive study of anti-triplet charmed baryon two-body decays. A comprehensive and intuitive analysis can be performed by introducing the topological diagrammatic approach (TDA), which provides clearer physical insights.

In fact, the two different methods (IRA and TDA) are mutually equivalent, as thoroughly analyzed in Refs. [18, 27, 53]. In our work, we adopt the same notation for the

TABLE II: The fit results for the real (Case I), complex (Case II), new (Case III) and TDA form factors.

form factors	Case I ($\chi^2/\text{d.o.f}=28.49/18=1.58$)				
vector(f)	$f^a = 0.0103(27)$	$f_6^b = 0.0193(47)$	$f_6^c = 0.0234(42)$	$f_6^d = -0.0090(40)$	$f^{a'} = 0.0007(73)$
	$f_{15}^b = -0.0103(25)$	$f_{15}^c = 0.0065(43)$	$f_{15}^d = -0.0154(22)$	$f_{15}^e = 0.0530(41)$	
axial-vector(g)	$g^a = -0.0295(79)$	$g_6^b = -0.1767(57)$	$g_6^c = 0.0896(90)$	$g_6^d = -0.0614(73)$	$g^{a'} = 0.025(44)$
	$g_{15}^b = 0.0739(49)$	$g_{15}^c = 0.0024(89)$	$g_{15}^d = -0.0150(59)$	$g_{15}^e = 0.0170(36)$	
form factors	Case II ($\chi^2/\text{d.o.f}=4.07/3=1.36$)				
	absolute value			strong phase	
vector(f)	$f^a = 0.039(29)$	$f_6^b = 0.007(48)$	$f_6^c = 0.022(9.63)$	$\delta f_6^b = -2.356(1.179)$	$\delta f_6^c = 2.035(209)$
	$f_6^d = 0.007(38)$	$f^{a'} = 0.014(13.97)$		$\delta f_6^d = 2.467(1.435)$	$\delta f^{a'} = -2.304(3.143)$
	$f_{15}^b = 0.032(79)$	$f_{15}^c = 0.004(9.63)$		$\delta f_{15}^b = 1.190(1.916)$	$\delta f_{15}^c = -1.816(1.621)$
	$f_{15}^d = 0.023(33)$	$f_{15}^e = 0.045(158)$		$\delta f_{15}^d = -1.347(935)$	$\delta f_{15}^e = -3.141(6.236)$
axial-vector(g)	$g^a = 0.120(368)$	$g_6^b = 0.110(284)$		$\delta g^a = -3.125(1.665)$	$\delta g_6^b = 0.027(642)$
	$g_6^c = 0.021(14.47)$	$g_6^d = 0.042(121)$		$\delta g_6^c = 1.907(3.802)$	$\delta g_6^d = -0.802(2.562)$
	$g^{a'} = 0.099(707)$			$\delta g^{a'} = -1.153(342)$	
	$g_{15}^b = 0.17(425)$	$g_{15}^c = 0.045(14.47)$		$\delta g_{15}^b = 2.061(2.209)$	$\delta g_{15}^c = 1.107(1.444)$
	$g_{15}^d = 0.056(175)$	$g_{15}^e = 0.008(126)$		$\delta g_{15}^d = -3.053(508)$	$\delta g_{15}^e = 1.546(4.42)$
form factors	Case III ($\chi^2/\text{d.o.f}=7.03/7=1.004$)				
	real part			imaginary part	
vector(f)	$f^a = -0.0289(61)$	$f_6^c = 0.010(10)$	$f_6^d = -0.008(17)$	$f_{T_1} = -0.0176(37)$	$f_{T_4} = -0.0019(81)$
	$f^{a'} = -0.01(50)$	$\text{Re}(\mathbf{f}_6^S) = 0.0003(114)$	$\text{Re}(\mathbf{f}_6^P) = 0.000051(40)$	$\text{Im}(\mathbf{f}_6^S) = -0.0105(36)$	$\text{Im}(\mathbf{f}_6^P) = -0.000049(80)$
	$f_{15}^b = 0.0326(72)$	$f_{15}^c = -0.0038(59)$	$f_{15}^d = -0.004(16)$	$f_{T_6} = -0.0192(71)$	$f_{T_7} = 0.031(12)$
	$f_{15}^e = -0.0338(76)$				
axial-vector(g)	$g^a = -0.014(18)$	$g_6^b = 0.083(41)$	$g_6^c = -0.023(39)$	$g_{T_1} = -0.016(18)$	$g_{T_3} = -0.08(1.52)$
	$g_6^d = 0.031(21)$	$g^{a'} = 0.05(49)$		$g_{T_4} = 0.068(36)$	$g_{T_6} = 0.031(26)$
	$g_{15}^b = -0.153(31)$	$g_{15}^c = -0.006(26)$	$g_{15}^d = -0.029(13)$	$g_{T_7} = -0.039(47)$	
	$g_{15}^e = -0.016(20)$				
form factors	TDA				
	T_1	T_2	T_3	T_4	T_5
vector(f)	$f_1 = 0.0813(47)$	$f_2 = 0.0247(58)$	$f_3 = -0.0052(14)$	$f_4 = -0.0084(11)$	$f_7 = 0.0149(41)$
	$f_{15} = 0.0406(24)$	$f_{16} = 0.0123(29)$	$f_5 = 0.0003(36)$	$f_6 = -0.0527(42)$	$f_8 = -0.0156(40)$
			$f_9 = 0.0055(38)$	$f_{10} = -0.0443(44)$	$f_{11} = -0.0305(59)$
	T_6	T_7			
axial-vector(g)	$f_{12} = 0.0234(42)$	$f_{17} = 0.0271(18)$			
	$f_{13} = -0.0252(33)$	$f_{18} = 0.0361(41)$			
	$f_{14} = -0.0486(36)$	$f_{19} = -0.0090(40)$			
	T_6	T_7			
axial-vector(g)	$g_1 = -0.0982(86)$	$g_2 = 0.1323(77)$	$g_3 = 0.0147(39)$	$g_4 = -0.0436(31)$	$g_7 = 0.0460(84)$
	$g_{15} = -0.0491(43)$	$g_{16} = 0.0662(38)$	$g_5 = 0.012(22)$	$g_6 = 0.026(12)$	$g_8 = -0.058(14)$
			$g_9 = -0.002(22)$	$g_{10} = 0.070(11)$	$g_{11} = -0.104(15)$
	T_6	T_7			
axial-vector(g)	$g_{12} = 0.0896(90)$	$g_{17} = -0.0591(37)$			
	$g_{13} = 0.052(14)$	$g_{18} = 0.0023(58)$			
	$g_{14} = -0.037(13)$	$g_{19} = -0.0614(73)$			
	T_6	T_7			

TDA amplitudes, denoted as $\bar{a}_{1\sim 19}$, following Ref. [18] as

$$\begin{aligned}
\mathcal{M}^{TDA} = & \bar{a}_1 T_{c3}^{[ij]} H_m^{kl}(\bar{T}_8)_{ijk} P_l^m \\
& + \bar{a}_2 T_{c3}^{[ij]} H_m^{kl}(\bar{T}_8)_{ijl} P_k^m + \bar{a}_3 T_{c3}^{[ij]} H_i^{kl}(\bar{T}_8)_{jkl} P_m^m \\
& + \bar{a}_4 T_{c3}^{[ij]} H_i^{kl}(\bar{T}_8)_{jkm} P_l^m + \bar{a}_5 T_{c3}^{[ij]} H_i^{kl}(\bar{T}_8)_{jlk} P_m^m \\
& + \bar{a}_6 T_{c3}^{[ij]} H_i^{kl}(\bar{T}_8)_{jmk} P_l^m + \bar{a}_7 T_{c3}^{[ij]} H_i^{kl}(\bar{T}_8)_{jlm} P_k^m \\
& + \bar{a}_8 T_{c3}^{[ij]} H_i^{kl}(\bar{T}_8)_{jml} P_k^m + \bar{a}_9 T_{c3}^{[ij]} H_i^{kl}(\bar{T}_8)_{klj} P_m^m
\end{aligned}$$

$$\begin{aligned}
& + \bar{a}_{10} T_{c3}^{[ij]} H_i^{kl}(\bar{T}_8)_{kmj} P_l^m + \bar{a}_{11} T_{c3}^{[ij]} H_i^{kl}(\bar{T}_8)_{lmj} P_k^m \\
& + \bar{a}_{12} T_{c3}^{[ij]} H_i^{kl}(\bar{T}_8)_{klm} P_j^m + \bar{a}_{13} T_{c3}^{[ij]} H_i^{kl}(\bar{T}_8)_{kml} P_j^m \\
& + \bar{a}_{14} T_{c3}^{[ij]} H_i^{kl}(\bar{T}_8)_{lmk} P_j^m + \bar{a}_{15} T_{c3}^{[ij]} H_m^{kl}(\bar{T}_8)_{ikj} P_l^m \\
& + \bar{a}_{16} T_{c3}^{[ij]} H_m^{kl}(\bar{T}_8)_{ilj} P_k^m + \bar{a}_{17} T_{c3}^{[ij]} H_m^{kl}(\bar{T}_8)_{ikl} P_j^m \\
& + \bar{a}_{18} T_{c3}^{[ij]} H_m^{kl}(\bar{T}_8)_{ilk} P_j^m + \bar{a}_{19} T_{c3}^{[ij]} H_m^{kl}(\bar{T}_8)_{klj} P_i^m (10)
\end{aligned}$$

The corresponding topological diagrams are illustrated in Fig. 1 ($T_1 \sim T_7$).

Using the definition $(T_8)_{ijk} = \epsilon_{ijl}(\bar{T}_8)_k^l$, the H_k^{ij} in TDA can be decomposed into IRA forms as

$$H_k^{ij} = \frac{1}{2} \left[(H_{15})_k^{ij} + \frac{1}{2} \epsilon^{ijl} (H_{\bar{6}})_{kl} \right]. \quad (11)$$

The transformation from TDA to IRA occurs naturally with the following relations for the parameters:

$$\begin{aligned} \bar{a}_1 &= b_6 - d_6 + e_{15}, & \bar{a}_2 &= d_6 - b_6 + e_{15}, & \bar{a}_3 &= -\frac{a}{2}, \\ \bar{a}_4 &= \frac{1}{2}(-c_6 + c_{15}), & \bar{a}_5 &= \frac{1}{2}a', & \bar{a}_7 &= \frac{1}{2}(c_6 + c_{15}), \\ \bar{a}_6 &= \frac{1}{2}(-b_6 - c_6 - e_{15} + d_{15}) + \frac{1}{4}(a + a'), \\ \bar{a}_8 &= \frac{1}{2}(b_6 + c_6 + d_{15} - e_{15}) - \frac{1}{4}(a + a'), \\ \bar{a}_9 &= \frac{1}{2}(a + a'), & \bar{a}_{12} &= c_6, & \bar{a}_{15} &= \frac{1}{2}(b_6 - d_6 + e_{15}), \\ \bar{a}_{10} &= \frac{1}{2}(-b_6 - c_{15} + d_{15} - e_{15}) + \frac{1}{4}(a + a'), \\ \bar{a}_{11} &= \frac{1}{2}(b_6 - c_{15} + d_{15} - e_{15}) - \frac{1}{4}(a + a'), \\ \bar{a}_{13} &= \frac{1}{2}(-e_{15} + b_{15} + c_6 + d_{15}) - \frac{1}{4}(a' - a) \\ \bar{a}_{14} &= \frac{1}{2}(-e_{15} + b_{15} - c_6 + d_{15}) - \frac{1}{4}(a' - a) \\ \bar{a}_{16} &= \frac{1}{2}(-b_6 + d_6 + e_{15}), & \bar{a}_{17} &= \frac{1}{2}(d_6 + e_{15} - b_{15}), \\ \bar{a}_{18} &= \frac{1}{2}(-d_6 + e_{15} - b_{15}), & \bar{a}_{19} &= d_6. \end{aligned} \quad (12)$$

By using the definition $\bar{a}_i = G_F \bar{u}(f_i - g_i \gamma_5)u$ with $i = 1 \sim 19$, the numerical results of the form factors for TDA are presented in the lower panel of Table. II. Since the form factors fitted in case II have significant uncertainty, we rely on the form factors fitted in case I for the numerical analysis.

Note that although diagrams T_1 to T_2 and T_4 to T_5 share similar topological structures, they differ in TDA due to the distinct contributions from operators O_1 and O_2 . As demonstrated in Ref. [18], each topological diagram in Fig. 1 corresponds to more than one TDA amplitude. Therefore, it is assumed that the absolute values of the TDA amplitudes with the same topological diagram should be equal. By defining the form factor $\mathcal{M}_{T_i} = G_F \bar{u}(f_{T_i} - g_{T_i} \gamma_5)u$, $i = 1 \sim 7$, one obtains the relations as

$$\begin{aligned} |A_{1,15}| &= A_{T_1}, & |A_{2,16}| &= A_{T_2}, & |A_{3,5,9}| &= A_{T_3}, \\ |A_{4,6,10}| &= A_{T_4}, & |A_{7,8,11}| &= A_{T_5}, \\ |A_{12,13,14}| &= A_{T_6}, & |A_{17,18,19}| &= A_{T_7}, & A &= f, g. \end{aligned} \quad (13)$$

The assumptions are approximately supported by the numerical results within 1σ in Table. II, which shows that the diagrams $T_{1,2}$ actually give the main contribution.

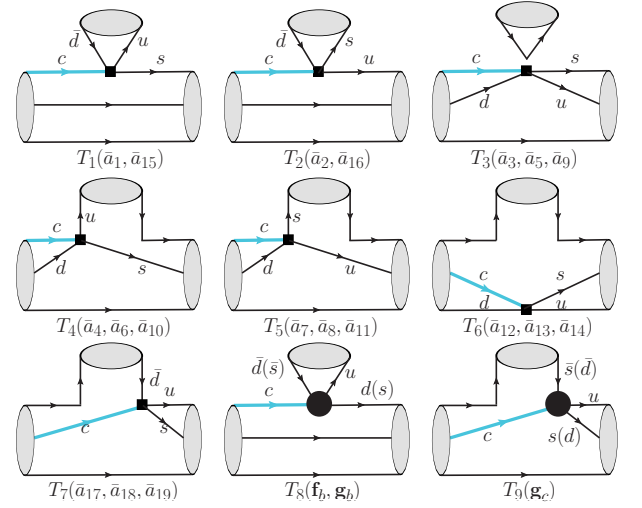


FIG. 1: Topology diagrams for the charmed baryon two body decays. Here T_{1-7} corresponding to the TDA amplitude in Eq.10. The Cabibbo-suppressed $c \rightarrow u\bar{d}d(\bar{s}s)$ and doubly-suppressed $c \rightarrow u\bar{s}d$ can be obtained similarly. $T_{8,9}$ describe the new effects in the Cabibbo-suppressed $c \rightarrow u\bar{d}d(\bar{s}s)$ induced by \mathbf{f}_b , \mathbf{g}_b and \mathbf{g}_c respectively.

However, some form factors contradict the assumption, such as $|f_{T_{17,18}}| - |f_{19}| \sim 0.02$ and $|g_{17,19}| - |g_{18}| \sim 0.05$. To focus on the largest effects, we ignore the discrepancy involving f_{19} and primarily consider $|g_{17,19}| > |g_{18}|$ in the subsequent analysis and this implies that there are other effects in the topology diagrams. Besides, since the difference of $T_1 - T_2$ and $T_4 - T_5$ contribution come from the operator O_1 and O_2 , one can expect that $A_{T_1}/A_{T_2} \approx A_{T_4}/A_{T_5}$. However, our numerical results conflict with it. We find the difference of contribution of diagram T_1 and T_2 is as large as $|f_{1,15}| - |f_{2,16}| \sim 0.06$, $|g_{T_2}| - |g_{T_1}| \sim 0.04$. The contributions of diagrams T_4 and T_5 are consistent within a 2σ standard deviation. This conflict make it reasonable to introduce a new form factor to account for the difference between T_1 and T_2 , while assuming $A_{T_4} = A_{T_5}$, where $A = f, g$.

For exploring the possible new effects, one defines the form factors \mathbf{f}_b and $\mathbf{g}_{b,c}$ to absorb these effect as $\mathbf{f}_b = f_{T_1} - f_{T_2}$, $\mathbf{g}_b = g_{T_1} - g_{T_2}$ and $\mathbf{g}_c = -g_{18} - g_{T_7}$. The corresponding topology diagrams $T_{8,9}$ are given in Fig. 1. Then the IRA form factors are expressed by TDA form

factors and $\mathbf{f}_b, \mathbf{g}_{b,c}$ as

$$\begin{aligned}
f^a &= -\frac{f_{T_6}}{2}, & f^{a'} &= \frac{1}{2}f_{T_6} - f_{T_3}, & f_b^b &= \frac{3}{2}\mathbf{f}_b, \\
f_{15}^b &= -f_{T_6} - f_{T_7}, & f_6^c &= f_{T_6} + f_{T_4}, & f_{15}^c &= f_{T_4}, \\
f_6^d &= -\frac{3}{2}\mathbf{f}_b - f_{T_7}, & f_{15}^d &= -2f_{T_4} - f_{T_6}, \\
f_{15}^e &= -\frac{3}{2}\mathbf{f}_b + 3f_{T_1} + 2f_{T_4} + f_{T_6} + f_{T_7}, \\
g^a &= g_{T_4} + \frac{g_{T_6}}{2}, & g^{a'} &= g_{T_4} + g_{T_3} - \frac{g_{T_6}}{2}, & g_{15}^c &= 0 \\
g_b^b &= -3g_{T_1} + \frac{3}{2}\mathbf{g}_b - 2g_{T_4}, & g_{15}^b &= \frac{\mathbf{g}_c}{2} + g_{T_6} + g_{T_7}, \\
g_6^c &= g_{T_6}, & g_6^d &= 3g_{T_1} - \frac{3}{2}\mathbf{g}_b - g_{T_7} + \frac{\mathbf{g}_c}{2}, & g_{15}^d &= g_{T_6}, \\
g_{15}^e &= -g_{T_6} - g_{T_7} - \frac{\mathbf{g}_c}{2} - \frac{3}{2}\mathbf{g}_b.
\end{aligned} \tag{14}$$

By adding the new form factor, the TDA form factor and IRA form factor become numerically equivalent. For example, in Eq. 14, without the new form factor, the IRA form factors f_6^b and g_{15}^c should be zero. Although the IRA form factor $g_{15}^c = 0.0024(89)$ we fitted is close to zero, $f_6^b = 0.0193(47)$ conflicts with our equivalence analysis. With the help of the new form factor \mathbf{f}_b , our fitted results align with the equivalence analysis above.

Although the new form factor we added can explain the equivalence of TDA and IRA amplitudes, the origin of these new form factors still needs further investigation. Since the diagrams T_8 and T_9 , corresponding to the new form factors, share the same topological structure as the diagrams induced by $O_{1,2}$ in TDA diagrams T_{1-7} , it is reasonable to conclude that these diagrams $T_{8,9}$ arise from SU(3) symmetry breaking. It is also evident that the penguin operators O_{3-6} can contribute to the diagrams T_1 and T_7 , but these contributions cannot be directly accounted for in the nine IRA amplitudes outlined in Eq. 4. Thus, the penguin operators can also contribute to the new form factors we introduced. In addition to these two possible sources, various other effects may also contribute to the formation of these new form factors. These contributions will be explored in detail in the subsequent section.

IV. CPV ANALYSIS UNDER SOME SCENARIOS

In the above analysis, we present an analysis using the SU(3) invariant representation (IRA) method for anti-triplet charmed baryon two-body decays. By incorporating the complex form factors, the nine IRA amplitudes can accurately reproduce the current experimental data. The fitted phase of the form factor enables the study of CP violation (CPV) effects. However, in previous work [50], the complex form factor in the IRA method, with contributions from the penguin diagram, introduces 51 parameters, which cannot be determined

with the current 37 experimental data. In our work, based on the analysis of the equivalence between TDA and IRA, we can predict the CP violation (CPV) under certain scenarios.

The above analysis shows that the IRA form factors with complex phases will introduce 35 parameters in our fit. To reduce the number of parameters, we can determine the strong phase from the perspective of topological diagrams, under the assumption that the imaginary part of the form factor in Eq. 13, corresponding to each topological diagram in Fig.1, is equal. Since the strong phase originates from the potential contributions of intermediate on-shell states in the decay process [48], this assumption appears to be reasonable. In this analysis, we further assume $\mathcal{I}m(f_{T_3}) = 0$ due to the global phase.

Since the new form factor may introduce a new weak phase, the CPV of the anti-triplet charmed baryon two-body decays can be studied under the assumption that the new weak phase is solely caused by the new form factors. To investigate CP violation (CPV), the potential origins of the new form factor are analyzed. The form factor \mathbf{f}/\mathbf{g}_b arises from the difference between topological diagrams T_1 and T_2 , which have distinct color structures shown in Fig. 1. The most likely source is the non-factorizable QCD contribution. The SU(3) symmetry breaking effect could also be the source, as the new form factor reveals the discrepancy between the SU(3) analysis methods: TDA and IRA. Particularly, when long-distance interactions influence the interaction vertex in Fig. 1, the flavor symmetry breaking effect is inevitably involved. Furthermore, final state rescattering (FSR) is anticipated to play a significant role in the new form factor, as these effects are not included in the IRA amplitude. Recent studies indicate that final state rescattering effects play a significant role in determining the magnitude of CP asymmetries in charmed hadron decay processes [46, 54]. Since it can contribute to topological diagrams involving singly Cabibbo-suppressed processes, final state rescattering is likely a potential source of the new form factor. In addition, the penguin operator can also contribute to the new form factor \mathbf{f}_b . Under flavor symmetry, the difference in the Lorentz structure at the Hamiltonian vertex can be ignored. Consequently, the penguin operator has the same Hamiltonian matrix structure as $O_{1,2}$ in TDA. In IRA, the penguin operator only contributes to H_3 , which we neglect in our analysis. Consequently, the new form factor \mathbf{f}_b , arising from the conflicting parts of IRA and TDA, must be accounted for. Since multiple potential sources could lead to new form factors, our approach is not restricted to a single CP violation (CPV) origin. We will examine all possible sources and incorporate the new form factors into our fit, performing a numerical analysis to assess its impact.

Based on the potential origins of these new form factors, their contributions can be estimated by referring to previous studies. The contribution of the penguin operator is found to be less than 10% [28, 50]. Although there are many indications suggesting SU(3) symmetry-

TABLE III: The predicted values for branching ratios, polarization parameters (α, β, γ) and CP violation with the final states $\eta^{(\prime)}$ for different fits. Case I(II)[III] means the fit results for the real(complex)[new] form factors.

channel	Case I		Case II				Case III
	Br(%)	α	Br(%)	α	β	γ	CPV
$\Lambda_c^+ \rightarrow \Sigma^+ \eta$	0.299(47)	-0.989(29)	0.32(5)	-0.985(60)	-0.1(1.3)	0.08(2.33)	
$\Lambda_c^+ \rightarrow \Sigma^+ \eta'$	0.428(66)	-0.467(64)	0.407(80)	-0.460(67)	-0.4(1.9)	0.8(1.1)	
$\Lambda_c^+ \rightarrow p \eta$	0.1583(97)	0.865(94)	0.158(11)	0.3(5)	-0.5(2.5)	-0.8(1.4)	-0.00058(88)
$\Lambda_c^+ \rightarrow p \eta'$	0.0484(61)	-0.992(15)	0.0488(91)	-0.28(60)	-0.85(76)	0.4(1.6)	0.0017(30)
$\Xi_c^+ \rightarrow \Sigma^+ \eta$	0.114(14)	0.88(15)	0.164(76)	0.7(2.1)	-0.7(1.8)	0.07(2.43)	-0.0008(17)
$\Xi_c^+ \rightarrow \Sigma^+ \eta'$	0.118(17)	-0.414(72)	0.060(48)	-0.9(1.2)	-0.4(4.1)	0.2(3.0)	0.0016(26)
$\Xi_c^+ \rightarrow p \eta$	0.00839(64)	-0.058(63)	0.012(11)	-0.68(73)	-0.69(87)	-0.26(78)	
$\Xi_c^+ \rightarrow p \eta'$	0.0092(10)	-0.993(11)	0.0060(47)	-0.68(58)	-0.73(98)	0.1(2.9)	
$\Xi_c^0 \rightarrow \Xi^0 \eta$	0.163(29)	0.98(16)	0.1(46.3)	-0.08(496.29)	0.7(211.9)	0.7(242.3)	
$\Xi_c^0 \rightarrow \Xi^0 \eta'$	0.116(33)	0.89(46)	0.09(29.53)	-0.5(145.5)	-0.2(756.2)	0.8(133.0)	
$\Xi_c^0 \rightarrow \Sigma^0 \eta$	0.0200(48)	0.83(22)	0.01(2.40)	0.5(274.5)	0.7(265.0)	0.5(196.4)	-0.0007(43)
$\Xi_c^0 \rightarrow \Sigma^0 \eta'$	0.0068(16)	0.67(68)	0.006(4.432)	-0.8(374.1)	0.2(545.0)	0.6(373.0)	0.0015(50)
$\Xi_c^0 \rightarrow \Lambda \eta$	0.0136(40)	0.94(14)	0.03(2.09)	-0.4(187.5)	0.9(66.8)	0.06(62.55)	-0.0018(91)
$\Xi_c^0 \rightarrow \Lambda \eta'$	0.0051(53)	0.94(70)	0.02(14.18)	-0.05(346.33)	-0.7(213.3)	0.7(222.3)	0.0004(1578)
$\Xi_c^0 \rightarrow n \eta$	0.00053(30)	-0.19(27)	0.002(283)	-0.7(312.9)	0.5(349.6)	-0.5(103.8)	
$\Xi_c^0 \rightarrow n \eta'$	0.00033(20)	0.96(57)	0.0002(381)	-0.04(1700)	-1(78)	0.1(379.8)	

breaking effects in charmed baryon decays, the previous global fit still shows that the symmetry-breaking effect is negligible within its error margins [55]. Regarding the FSR, recent studies suggest that the strong phase in the parity-conserving form factor related to FSR is nearly zero [46]. Therefore, in our work, we can neglect the imaginary component of the parity-conserving new form factor as $\mathcal{I}m(\mathbf{g}_{b/c}) = 0$, since $\mathbf{g}_{b/c}$ appears in conjunction with other TDA form factors. However, the new form factor \mathbf{f}_b exclusively contributes to the IRA form factor f_6^b , suggesting that its contribution cannot be ignored.

According to the above analysis, the new form factor can be expressed as

$$\mathbf{f}_b = \mathbf{f}_b^S + \mathbf{f}_b^P e^{i\phi^P}, \quad (15)$$

where \mathbf{f}_b^S is derived from SU(3) symmetry breaking and non-factorizable QCD contributions, which do not produce a weak phase. The term $\mathbf{f}_b^P e^{i\phi^P}$ represents the contribution from the penguin operator and final state radiation (FSR) effects, with the weak phase $\phi^P = -1.147 \pm 0.026$. The form factors in our global analy-

sis are expressed as:

$$\begin{aligned} A_{6,15}^q &= e^{i\phi_1} \left(\mathcal{R}e(A_{6,15}^q) + \mathcal{I}m(A_{6,15}^q) \right), \\ f_6^b &= \frac{3}{2} \left(e^{i\phi_1} (\mathcal{R}e(\mathbf{f}_b^S) + \mathcal{I}m(\mathbf{f}_b^S)) \right. \\ &\quad \left. + e^{i\phi^P} (\mathcal{R}e(\mathbf{f}_b^P) + \mathcal{I}m(\mathbf{f}_b^P)) \right), \\ f_6^d &= e^{i\phi_1} (\mathcal{R}e(f_6^d) + \mathcal{I}m(f_6^d)) \\ &\quad - e^{i\phi^P} \frac{3}{2} (\mathcal{R}e(\mathbf{f}_b^P) + \mathcal{I}m(\mathbf{f}_b^P)), \\ f_{15}^e &= e^{i\phi_1} (\mathcal{R}e(f_{15}^e) + \mathcal{I}m(f_{15}^e)) \\ &\quad - e^{i\phi^P} \frac{3}{2} (\mathcal{R}e(\mathbf{f}_b^P) + \mathcal{I}m(\mathbf{f}_b^P)), \quad A = f, g, \quad (16) \end{aligned}$$

where $q = a, b, c, d, e$. The weak phase ϕ_1 arises from the current-current operator as $\phi_1 = \arg(V_{cq}^* V_{uq'}) \approx 0, -\pi$. One can find that the penguin operator only contribute to the Cabibbo-suppressed processes. The SU(3) symmetry requires the form factor corresponding to different processes to be equal [26, 27], one has the chance to determine the form factor \mathbf{f}_b^S by the Cabibbo-allowed and doubly Cabibbo-suppressed processes. Based on the symmetry breaking form factor we derived, the penguin contribution form factor \mathbf{f}_b^P can be further determined by the Cabibbo-suppressed processes.

By introducing the weak phase of penguin operator ϕ^T , one can derive the CPV if the global fit gives a nonzero value of \mathbf{f}_b^P . In our analysis, we obtains the fit results with $\chi^2/d.o.f = 1.004$, indicating that our fit is reasonable and the form factors effectively explain the experimental

TABLE IV: The predicted values for branching ratios, polarization parameters (α, β, γ) and CP violation for different fits. Case I(II)[III] means the fit results for the real(complex)[new] form factors.

channel	Case I		Case II				Case III
	Br(%)	α	Br(%)	α	β	γ	CPV
$\Lambda_c^+ \rightarrow \Sigma^0 \pi^+$	1.248(46)	-0.472(15)	1.245(48)	-0.472(15)	-0.88(13)	-0.09(1.21)	
$\Lambda_c^+ \rightarrow \Lambda \pi^+$	1.309(47)	-0.7536(60)	1.272(48)	-0.7551(60)	0.58(46)	0.30(89)	
$\Lambda_c^+ \rightarrow \Sigma^+ \pi^0$	1.262(42)	-0.470(15)	1.253(48)	-0.471(15)	-0.88(13)	-0.1(1.2)	
$\Lambda_c^+ \rightarrow p K_S^0$	1.581(47)	0.39(14)	1.580(69)	-0.05(38)	-0.8(1.6)	-0.6(1.9)	
$\Lambda_c^+ \rightarrow \Xi^0 K^+$	0.423(29)	0.957(18)	0.555(70)	0.04(15)	0.37(88)	0.93(36)	
$\Xi_c^+ \rightarrow \Sigma^+ K_S^0$	0.81(21)	0.63(19)	0.9(2.0)	0.81(35)	0.3(2.0)	0.49(97)	
$\Xi_c^+ \rightarrow \Xi^0 \pi^+$	0.875(77)	-0.900(38)	1.94(59)	0.20(17)	0.4(1.2)	0.91(45)	
$\Xi_c^0 \rightarrow \Sigma^0 K_S^0$	0.054(16)	-0.41(29)	0.055(16)	0.4(645.1)	0.7(482.9)	0.6(526.4)	
$\Xi_c^0 \rightarrow \Lambda K_S^0$	0.225(34)	0.88(18)	0.324(60)	-0.4(250.9)	0.9(109.4)	-0.1(121.6)	
$\Xi_c^0 \rightarrow \Sigma^+ K^-$	0.195(39)	0.87(33)	0.181(40)	0.9(326)	-0.07(1200)	-0.5(443.2)	
$\Xi_c^0 \rightarrow \Xi^- \pi^+$	1.16(18)	-0.709(45)	1.18(19)	-0.640(51)	-0.76(10)	-0.08(89)	
$\Xi_c^0 \rightarrow \Xi^0 \pi^0$	0.152(48)	-0.45(13)	0.68(14)	-0.87(28)	0.39(53)	-0.31(82)	
$\Lambda_c^+ \rightarrow \Sigma^0 K^+$	0.0377(18)	-0.9960(42)	0.0389(25)	-0.58(16)	-0.2(1.1)	-0.79(34)	0.0015(18)
$\Lambda_c^+ \rightarrow \Lambda K^+$	0.0639(29)	-0.547(44)	0.0645(31)	-0.585(49)	-0.08(91)	0.806(99)	0.0011(13)
$\Lambda_c^+ \rightarrow \Sigma^+ K_{S,L}^0$	0.0277(27)	-0.69(10)	0.042(13)	-0.81(46)	-0.53(62)	0.26(71)	-0.0004(46)
$\Lambda_c^+ \rightarrow p \pi^0$	0.0163(60)	-0.16(13)	0.0158(75)	0.7(4.3)	-0.6(4.5)	0.4(1.2)	
$\Lambda_c^+ \rightarrow n \pi^+$	0.0642(23)	0.539(43)	0.0766(88)	0.10(17)	0.5(1.6)	0.88(83)	-0.0052(39)
$\Xi_c^+ \rightarrow \Sigma^0 \pi^+$	0.3161(88)	-0.729(17)	0.254(13)	-0.902(31)	-0.35(34)	0.25(47)	
$\Xi_c^+ \rightarrow \Lambda \pi^+$	0.0218(32)	-0.16(18)	0.095(10)	0.43(31)	0.52(69)	-0.74(56)	-0.0005(32)
$\Xi_c^+ \rightarrow \Sigma^+ \pi^0$	0.288(19)	0.40(13)	0.263(94)	0.27(56)	-0.7(1.3)	-0.6(1.4)	-0.00027(85)
$\Xi_c^+ \rightarrow p K_{S,L}^0$	0.144(14)	-0.495(86)	0.155(24)	-0.83(42)	-0.54(65)	-0.14(75)	-0.0002(27)
$\Xi_c^+ \rightarrow \Xi^0 K^+$	0.1340(55)	0.376(33)	0.162(33)	0.07(11)	0.3(1.2)	0.94(39)	-0.0052(39)
$\Xi_c^0 \rightarrow \Sigma^0 \pi^0$	0.00007(22)	-0.5(2.3)	0.04(5.31)	-0.6(228.9)	0.8(151.0)	-0.2(173.1)	-0.0009(42)
$\Xi_c^0 \rightarrow \Lambda \pi^0$	0.0314(56)	0.71(12)	0.03(5.47)	-1(17)	-0.1(27.3)	-0.1(165.1)	0.0013(20)
$\Xi_c^0 \rightarrow \Sigma^+ \pi^-$	0.0123(26)	0.84(35)	0.01(33)	0.8(337.2)	-0.07(1200)	-0.6(412.1)	
$\Xi_c^0 \rightarrow p K^-$	0.0154(40)	0.73(38)	0.01(1.50)	0.7(349)	-0.06(1000)	-0.7(316.2)	
$\Xi_c^0 \rightarrow \Sigma^- \pi^+$	0.0625(97)	-0.778(44)	0.071(16)	-0.627(92)	-0.75(19)	-0.22(85)	
$\Xi_c^0 \rightarrow n K_{S,L}^0$	0.0201(50)	0.40(33)	0.02(81)	-0.4(507.4)	0.7(345.2)	-0.6(213.4)	-0.0031(43)
$\Xi_c^0 \rightarrow \Xi^- K^+$	0.0515(80)	-0.665(44)	0.0491(82)	-0.642(71)	-0.767(54)	0.007(894)	
$\Xi_c^0 \rightarrow \Xi^0 K_{S,L}^0$	0.0088(20)	0.58(43)	0.01(83)	-0.4(618.2)	0.9(346.5)	1(0)	-0.0051(66)
$\Lambda_c^+ \rightarrow p K_L^0$	1.689(49)	0.46(14)	1.677(69)	0.03(41)	-0.8(1.7)	-0.6(2.0)	
$\Lambda_c^+ \rightarrow n K^+$	0.001008(89)	-0.979(19)	0.00193(36)	0.25(25)	0.5(1.4)	0.85(71)	
$\Xi_c^+ \rightarrow \Sigma^0 K^+$	0.01142(30)	-0.9961(13)	0.01006(53)	-0.990(16)	0.12(13)	-0.07(25)	
$\Xi_c^+ \rightarrow \Lambda K^+$	0.00437(18)	0.620(30)	0.0047(10)	0.28(14)	-0.86(62)	0.4(1.2)	
$\Xi_c^+ \rightarrow \Sigma^+ K_L^0$	1.01(23)	0.82(15)	1.1(2.1)	0.95(21)	0.2(2.2)	0.3(1.0)	
$\Xi_c^+ \rightarrow p \pi^0$	0.00103(32)	0.10(26)	0.0014(27)	0.3(3.8)	0.2(1.9)	-0.9(1.5)	
$\Xi_c^+ \rightarrow n \pi^+$	0.00612(39)	0.942(20)	0.0045(19)	0.07(26)	0.7(1.3)	0.8(1.1)	
$\Xi_c^0 \rightarrow \Sigma^0 K_L^0$	0.069(18)	-0.14(29)	0.08(46)	0.3(583.5)	0.8(319.9)	0.6(423.3)	
$\Xi_c^0 \rightarrow \Lambda K_L^0$	0.211(31)	0.91(15)	0.31(15)	-0.4(207.9)	0.9(85.8)	-0.09(101.86)	
$\Xi_c^0 \rightarrow p \pi^-$	0.00092(25)	0.71(38)	0.0009(1009)	0.7(347.7)	-0.06(990)	-0.7(298.3)	
$\Xi_c^0 \rightarrow \Sigma^- K^+$	0.00282(44)	-0.744(44)	0.00305(56)	-0.635(65)	-0.76(15)	-0.15(87)	
$\Xi_c^0 \rightarrow n \pi^0$	0.00142(27)	0.998(18)	0.001(601)	-1(69)	0.2(87.3)	-0.09(525.77)	

data.

With the determined penguin operator contribution $\mathcal{R}e(\mathbf{f}_b^P) = 0.000051(40)$ and $\mathcal{I}m(\mathbf{f}_b^P) = -0.000049(80)$, one can predict the CP violation (A_{CP}) for the Cabibbo-suppressed processes. Considering the ratio of the form factor from current-current and penguin operator $\frac{\langle O_{1,2} \rangle}{\langle O_{3-6} \rangle} \sim O(10^{-2})$, our study implies that the contribution of the QCD penguin may be more substantial than conventionally assumed, necessitating further theoretical investigation in the future.

Based on the fitted results, we predict the values of A_{CP} for the Cabibbo-suppressed processes and find that almost all the predicted A_{CP} values are approximately zero within the errors, except for the following processes

$$\begin{aligned} A_{CP}^{\Lambda_c^+ \rightarrow n\pi^+} &= -0.0052(39), \\ A_{CP}^{\Xi_c^+ \rightarrow \Xi^0 K^+} &= -0.0052(39). \end{aligned} \quad (17)$$

We strongly recommend the experimental measurement of the processes: $\Lambda_c^+ \rightarrow n\pi^+$ since their branching ratio has been measured. Surprisingly, one can observe that the CPV we predicted for $\Lambda_c^+ \rightarrow n\pi^+$ and $\Xi_c^+ \rightarrow \Xi^0 K^+$ channels are equal. The identical CPV effects in the $\Lambda_c^+ \rightarrow n\pi^+$ and $\Xi_c^+ \rightarrow \Xi^0 K^+$ decay channels arise from their shared SU(3) decay amplitudes, expressed as $-\sin\theta(c_6 - c_{15} + d_6 + d_{15})$. Moreover, this analysis assumes that the new weak phase is introduced exclusively through the new form factor \mathbf{f}_b , thereby restricting CPV contributions to specific IRA form factors f_6^b , f_6^d , and f_6^e . Consequently, the amplitudes for these decay channels rely on the same combination, $d_6 + e_{15}$, which results in identical CPV effects. The CPV for other channels (case III) is summarized in Table. III and Table. IV.

V. CONCLUSION

In this study, we performed a global analysis of two-body decays of anti-triplet charmed baryons. Utilizing 35 experimental data points, we successfully determined 18 real IRA form factors, as shown in Table II (Case I). The branching ratios and polarization parameters (Case I) for these processes are presented in Table III and Table IV, respectively. Notably, the polarization parameters of $\Lambda_c^+ \rightarrow \Xi^0 K^+$ and $\Xi_c^0 \rightarrow \Xi^0 \pi^0$ show discrepancies when compared with our results, indicating the necessity of considering complex form factors.

Fortunately, by incorporating the complex 18 IRA form factors, the 35 parameters can be determined using a total of 37 experimental measurements. The fitted form factors and predictions (Case II) are provided in Table. II, Table. III, and Table. IV, respectively. Although

the low degrees of freedom result in large uncertainties, the $\chi^2/\text{d.o.f} = 1.36$ indicates that SU(3) symmetry is well-preserved.

Based on the form factors determined in the global fit (Case I), we analyze the equivalence between the SU(3) IRA and TDA methods. Our findings suggest that the results derived from the IRA method are largely consistent with the assumptions of the TDA method, as depicted in the topological diagram in Fig. 1. However, some form factors exhibit deviations from the predicted values based on the topological diagrams. To quantify these deviations, we introduce the form factors \mathbf{f}_b and $\mathbf{g}_{b/c}$ to represent the new effects.

Leveraging the newly introduced form factors, we aim to investigate the CPV effect under specific scenarios. Assuming that the imaginary part of the form factor in Eq. 13 is equal for each topological diagram in Fig.1, the number of parameters can be reduced to 31. Furthermore, assuming that the new weak phase arises solely from the new form factor, the CPV in anti-triplet charmed baryon two-body decays can be predicted. The fitted form factors and the predicted CPV values (case III) are presented in Table.II, Table.III, and Table.IV, respectively. Based on these assumptions, our analysis predicts non-zero A_{CP} in Eq. 17. Given its associated error, observable CP violation can be detected at the level of $O(10^{-3})$. We strongly recommend measuring these processes.

It is important to note that the most ideal condition for measuring CP violation is the simultaneous production of charmed baryon and anti-baryon pairs. The BESIII Collaborations meet these conditions, with extensive data on $\Lambda_c \bar{\Lambda}_c$ and $\Xi_c \bar{\Xi}_c$ pairs. For $\Lambda_c^+ \rightarrow n\pi^+$, the branching ratio has already been measured by the BESIII Collaborations. Therefore, this facility holds the potential to observe CP violation in charmed baryon decays for the first time.

ACKNOWLEDGEMENTS

We thank Prof. Xiao-Gang He, Prof. Wei Wang and Prof. YuJi Shi for useful discussion. The work of Jin Sun is supported by IBS under the project code, IBS-R018-D1. The work of Ruilin Zhu is supported by NSFC under grant No. 12322503 and No. 12075124, and by Natural Science Foundation of Jiangsu under Grant No. BK20211267. The work of Zhi-Peng Xing is supported by NSFC under grant No.12375088 and No. 12335003.

[1] Belle Collaboration, R. Mizuk *et al.*, “Observation of

an isotriplet of excited charmed baryons decaying to

- Lambda+(c) pi,” *Phys. Rev. Lett.* **94** (2005) 122002, arXiv:hep-ex/0412069.
- [2] Belle Collaboration, G. Pakhlova *et al.*, “Observation of a near-threshold enhancement in the $e^+e^- \rightarrow \Lambda_b^0 \Lambda_b^0$ cross section using initial-state radiation,” *Phys. Rev. Lett.* **101** (2008) 172001, arXiv:0807.4458 [hep-ex].
- [3] LHCb Collaboration, R. Aaij *et al.*, “Prompt charm production in pp collisions at $\sqrt{s}=7$ TeV,” *Nucl. Phys. B* **871** (2013) 1–20, arXiv:1302.2864 [hep-ex].
- [4] LHCb Collaboration, R. Aaij *et al.*, “Differential branching fraction and angular analysis of $\Lambda_b^0 \rightarrow \Lambda \mu^+ \mu^-$ decays,” *JHEP* **06** (2015) 115, arXiv:1503.07138 [hep-ex]. [Erratum: JHEP 09, 145 (2018)].
- [5] BESIII Collaboration, M. Ablikim *et al.*, “Measurement of the absolute branching fraction for $\Lambda_c^+ \rightarrow \Lambda e^+ \nu_e$,” *Phys. Rev. Lett.* **115** no. 22, (2015) 221805, arXiv:1510.02610 [hep-ex].
- [6] BESIII Collaboration, M. Ablikim *et al.*, “Measurements of absolute hadronic branching fractions of Λ_c^+ baryon,” *Phys. Rev. Lett.* **116** no. 5, (2016) 052001, arXiv:1511.08380 [hep-ex].
- [7] LHCb Collaboration, R. Aaij *et al.*, “Observation of five new narrow Ω_c^0 states decaying to $\Xi_c^+ K^-$,” *Phys. Rev. Lett.* **118** no. 18, (2017) 182001, arXiv:1703.04639 [hep-ex].
- [8] BESIII Collaboration, M. Ablikim *et al.*, “Precision measurement of the $e^+e^- \rightarrow \Lambda_c^+ \bar{\Lambda}_c^-$ cross section near threshold,” *Phys. Rev. Lett.* **120** no. 13, (2018) 132001, arXiv:1710.00150 [hep-ex].
- [9] Belle Collaboration, J. Yelton *et al.*, “Observation of Excited Ω_c Charmed Baryons in e^+e^- Collisions,” *Phys. Rev. D* **97** no. 5, (2018) 051102, arXiv:1711.07927 [hep-ex].
- [10] LHCb Collaboration, R. Aaij *et al.*, “First Observation of the Doubly Charmed Baryon Decay $\Xi_{cc}^{++} \rightarrow \Xi_c^+ \pi^+$,” *Phys. Rev. Lett.* **121** no. 16, (2018) 162002, arXiv:1807.01919 [hep-ex].
- [11] LHCb Collaboration, R. Aaij *et al.*, “Measurement of the Ω_c^0 baryon lifetime,” *Phys. Rev. Lett.* **121** no. 9, (2018) 092003, arXiv:1807.02024 [hep-ex].
- [12] W. Roberts and M. Pervin, “Heavy baryons in a quark model,” *Int. J. Mod. Phys. A* **23** (2008) 2817–2860, arXiv:0711.2492 [nucl-th].
- [13] R. A. Briceño, H.-W. Lin, and D. R. Bolton, “Charmed-Baryon Spectroscopy from Lattice QCD with $N_f = 2+1+1$ Flavors,” *Phys. Rev. D* **86** (2012) 094504, arXiv:1207.3536 [hep-lat].
- [14] O. Romanets, L. Tolos, C. Garcia-Recio, J. Nieves, L. L. Salcedo, and R. G. E. Timmermans, “Charmed and strange baryon resonances with heavy-quark spin symmetry,” *Phys. Rev. D* **85** (2012) 114032, arXiv:1202.2239 [hep-ph].
- [15] Z. S. Brown, W. Detmold, S. Meinel, and K. Orginos, “Charmed bottom baryon spectroscopy from lattice QCD,” *Phys. Rev. D* **90** no. 9, (2014) 094507, arXiv:1409.0497 [hep-lat].
- [16] C.-D. Lü, W. Wang, and F.-S. Yu, “Test flavor SU(3) symmetry in exclusive Λ_c decays,” *Phys. Rev. D* **93** no. 5, (2016) 056008, arXiv:1601.04241 [hep-ph].
- [17] X.-G. He and W. Wang, “Flavor SU(3) Topological Diagram and Irreducible Representation Amplitudes for Heavy Meson Charmless Hadronic Decays: Mismatch and Equivalence,” *Chin. Phys. C* **42** no. 10, (2018) 103108, arXiv:1803.04227 [hep-ph].
- [18] X.-G. He, Y.-J. Shi, and W. Wang, “Unification of Flavor SU(3) Analyses of Heavy Hadron Weak Decays,” *Eur. Phys. J. C* **80** no. 5, (2020) 359, arXiv:1811.03480 [hep-ph].
- [19] H. J. Zhao, Y.-L. Wang, Y. K. Hsiao, and Y. Yu, “A diagrammatic analysis of two-body charmed baryon decays with flavor symmetry,” *JHEP* **02** (2020) 165, arXiv:1811.07265 [hep-ph].
- [20] M. He and R. Rapp, “Charm-Baryon Production in Proton-Proton Collisions,” *Phys. Lett. B* **795** (2019) 117–121, arXiv:1902.08889 [nucl-th].
- [21] C. Q. Geng, C.-W. Liu, and T.-H. Tsai, “Asymmetries of anti-triplet charmed baryon decays,” *Phys. Lett. B* **794** (2019) 19–28, arXiv:1902.06189 [hep-ph].
- [22] C.-P. Jia, D. Wang, and F.-S. Yu, “Charmed baryon decays in $SU(3)_F$ symmetry,” *Nucl. Phys. B* **956** (2020) 115048, arXiv:1910.00876 [hep-ph].
- [23] D. Wang, C.-P. Jia, and F.-S. Yu, “A self-consistent framework of topological amplitude and its $SU(N)$ decomposition,” *JHEP* **21** (2020) 126, arXiv:2001.09460 [hep-ph].
- [24] F. Huang, Z.-P. Xing, and X.-G. He, “A global analysis of charmless two body hadronic decays for anti-triplet charmed baryons,” *JHEP* **03** (2022) 143, arXiv:2112.10556 [hep-ph]. [Erratum: JHEP 09, 087 (2022)].
- [25] Z.-P. Xing, X.-G. He, F. Huang, and C. Yang, “Global analysis of measured and unmeasured hadronic two-body weak decays of antitriplet charmed baryons,” *Phys. Rev. D* **108** no. 5, (2023) 053004, arXiv:2305.14854 [hep-ph].
- [26] C.-Q. Geng, X.-G. He, X.-N. Jin, C.-W. Liu, and C. Yang, “Complete determination of $SU(3)_F$ amplitudes and strong phase in $\Lambda_c^+ \rightarrow \Xi^0 K^+$,” *Phys. Rev. D* **109** no. 7, (2024) L071302, arXiv:2310.05491 [hep-ph].
- [27] H. Zhong, F. Xu, and H.-Y. Cheng, “Analysis of hadronic weak decays of charmed baryons in the topological diagrammatic approach,” *Phys. Rev. D* **109** no. 11, (2024) 114027, arXiv:2404.01350 [hep-ph].
- [28] D. Wang and J.-F. Luo, “Topological diagrams of charmed baryon decays in the $SU(3)_F$ limit,” arXiv:2406.14061 [hep-ph].
- [29] H.-Y. Cheng, F. Xu, and H. Zhong, “Hadronic Weak Decays of Charmed Baryons in the Topological Diagrammatic Approach: An Update,” arXiv:2410.04675 [hep-ph].
- [30] BESIII Collaboration, M. Ablikim *et al.*, “Evidence of the singly Cabibbo suppressed decay $\Lambda_c^+ \rightarrow p \pi^0$,” *Phys. Rev. D* **109** no. 9, (2024) L091101, arXiv:2311.06883 [hep-ex].

- [31] **Belle-II, Belle** Collaboration, I. Adachi *et al.*, “Measurements of the branching fractions of $\Xi_c^0 \rightarrow \Xi^0 \pi^0$, $\Xi_c^0 \rightarrow \Xi^0 \eta$, and $\Xi_c^0 \rightarrow \Xi^0 \eta'$ and asymmetry parameter of $\Xi_c^0 \rightarrow \Xi^0 \pi^0$,” [arXiv:2406.04642 \[hep-ex\]](#).
- [32] **BESIII** Collaboration, M. Ablikim *et al.*, “Measurements of K_S^0 - K_L^0 asymmetries in the decays $\Lambda_c^+ \rightarrow p K_{L,S}^0$, $p K_{L,S}^0 \pi^+ \pi^-$ and $p K_{L,S}^0 \pi^0$,” [arXiv:2406.18083 \[hep-ex\]](#).
- [33] **Belle-II, Belle** Collaboration, I. Adachi *et al.*, “Observations of the singly Cabibbo-suppressed decays $\Xi_c^+ \rightarrow p K_S^0$, $\Xi_c^+ \rightarrow \Lambda \pi^+$, and $\Xi_c^+ \rightarrow \Sigma^0 \pi^+$ at Belle and Belle II,” [arXiv:2412.10677 \[hep-ex\]](#).
- [34] T. D. Lee and C.-N. Yang, “General Partial Wave Analysis of the Decay of a Hyperon of Spin 1/2,” *Phys. Rev.* **108** (1957) 1645–1647.
- [35] M. Kobayashi and T. Maskawa, “CP Violation in the Renormalizable Theory of Weak Interaction,” *Prog. Theor. Phys.* **49** (1973) 652–657.
- [36] N. G. Deshpande and X.-G. He, “CP asymmetry relations between anti-b0 \rightarrow pi pi and anti-b0 \rightarrow pi K rates,” *Phys. Rev. Lett.* **75** (1995) 1703–1706, [arXiv:hep-ph/9412393](#).
- [37] **LHCb** Collaboration, R. Aaij *et al.*, “Observation of CP Violation in Charm Decays,” *Phys. Rev. Lett.* **122** no. 21, (2019) 211803, [arXiv:1903.08726 \[hep-ex\]](#).
- [38] A. Lenz and G. Wilkinson, “Mixing and CP Violation in the Charm System,” *Ann. Rev. Nucl. Part. Sci.* **71** (2021) 59–85, [arXiv:2011.04443 \[hep-ph\]](#).
- [39] S. Schacht and A. Soni, “Enhancement of charm CP violation due to nearby resonances,” *Phys. Lett. B* **825** (2022) 136855, [arXiv:2110.07619 \[hep-ph\]](#).
- [40] I. Bediaga, T. Frederico, and P. C. Magalhães, “Enhanced Charm CP Asymmetries from Final State Interactions,” *Phys. Rev. Lett.* **131** no. 5, (2023) 051802, [arXiv:2203.04056 \[hep-ph\]](#).
- [41] J.-P. Wang and F.-S. Yu, “Probing hyperon CP violation with charmed baryon decays,” *Phys. Lett. B* **849** (2024) 138460, [arXiv:2208.01589 \[hep-ph\]](#).
- [42] J.-P. Wang, Q. Qin, and F.-S. Yu, “CP violation induced by T-odd correlations and its baryonic application,” [arXiv:2211.07332 \[hep-ph\]](#).
- [43] **LHCb** Collaboration, S. Maccolini, “Mixing and CPV in charm decays at LHCb,” *PoS FPCP2023* (2023) 081.
- [44] Y.-F. Shen, J.-P. Wang, and Q. Qin, “Possible large CP violation in charmed Λ_b decays,” *Phys. Rev. D* **108** no. 11, (2023) L111901, [arXiv:2309.09854 \[hep-ph\]](#).
- [45] W.-J. Song, Y.-F. Shen, and Q. Qin, “Double-mixing CP violation in B decays,” [arXiv:2403.01904 \[hep-ph\]](#).
- [46] X.-G. He and C.-W. Liu, “Large CP violation in charmed baryon decays,” [arXiv:2404.19166 \[hep-ph\]](#).
- [47] S. Schacht, “Charm CP violation and searches,” in *58th Rencontres de Moriond on Electroweak Interactions and Unified Theories*. 5, 2024. [arXiv:2405.09299 \[hep-ph\]](#).
- [48] **Particle Data Group** Collaboration, S. N. et al., “Review of Particle Physics,” *to be published in Phys. Rev. D* **110** (2024) 030001.
- [49] L. Gan, B. Kubis, E. Passemar, and S. Tulin, “Precision tests of fundamental physics with η and η' mesons,” *Phys. Rept.* **945** (2022) 1–105, [arXiv:2007.00664 \[hep-ph\]](#).
- [50] Z.-P. Xing, Y.-J. Shi, J. Sun, and Y. Xing, “SU(3) symmetry analysis in charmed baryon two body decays with penguin diagram contribution,” [arXiv:2407.09234 \[hep-ph\]](#).
- [51] P. Lepage and C. Gohlke, “gplepage/lsgfit: lsgfit version 13.2.2(v13.2),zenodo doi.org/10.5281/zenodo.4037174,”.
- [52] **BESIII** Collaboration, M. Ablikim *et al.*, “First Measurement of the Decay Asymmetry in the Pure W-Boson-Exchange Decay $\Lambda_c^+ \rightarrow \Xi^0 K^+$,” *Phys. Rev. Lett.* **132** no. 3, (2024) 031801, [arXiv:2309.02774 \[hep-ex\]](#).
- [53] Y. K. Hsiao, Y. L. Wang, and H. J. Zhao, “Equivalent SU(3)_f approaches for two-body anti-triplet charmed baryon decays,” *JHEP* **09** (2022) 035, [arXiv:2111.04124 \[hep-ph\]](#).
- [54] C.-P. Jia, H.-Y. Jiang, J.-P. Wang, and F.-S. Yu, “Final-state rescattering mechanism of charmed baryon decays,” [arXiv:2408.14959 \[hep-ph\]](#).
- [55] X.-G. He, F. Huang, W. Wang, and Z.-P. Xing, “SU(3) symmetry and its breaking effects in semileptonic heavy baryon decays,” *Phys. Lett. B* **823** (2021) 136765, [arXiv:2110.04179 \[hep-ph\]](#).